

## Supplementary Information: Upper limit to the photovoltaic efficiency of imperfect crystals from first principles

Sunghyun Kim,<sup>1</sup> José A. Márquez,<sup>2</sup> Thomas Unold,<sup>2</sup> and Aron Walsh<sup>1,3</sup>

<sup>1</sup>Department of Materials, Imperial College London, Exhibition Road, London SW7 2AZ, UK

<sup>2</sup>Helmholtz-Zentrum Berlin für Materialien und Energie GmbH,  
 Department Structure and Dynamics of Energy Materials,  
 Hahn-Meitner-Platz 1, D-14109 Berlin, Germany

<sup>3</sup>Department of Materials Science and Engineering, Yonsei University, Seoul 03722, Korea\*

(Dated: March 9, 2020)

### METHODS

#### Computational steps for the trap-limited conversion efficiency

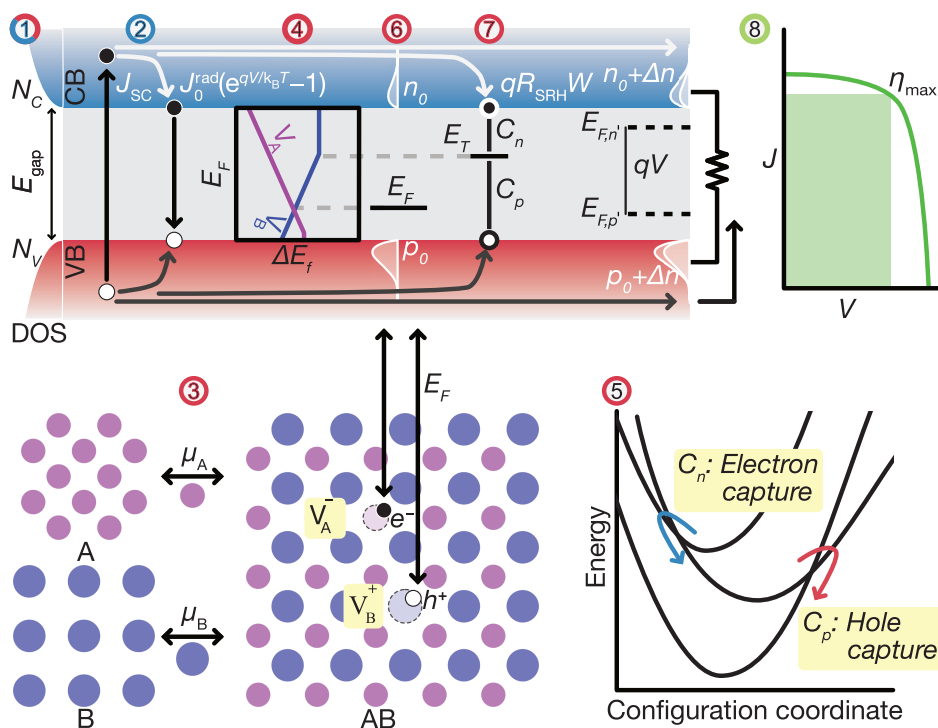


FIG. S1. **Diagram for the calculation of trap-limited conversion efficiency.** The physical processes that are considered to calculate the trap-limited conversion efficiency are drawn in terms of the electronic and the atomic structure. The numbered steps are the same as in Fig. 1 in the main text.

Step	Description	Parameters
1 Band structure	First-principles calculations can provide the electronic band structure.	$E_{\text{gap}}, N_C, N_V$
2 Radiative limit	The band gap (step 1) determines optical absorption, hot-carrier cooling, and radiative recombination. Based on the principle of detailed balance, the Shockley-Queisser (SQ) limit can predict the short-circuit current and radiative recombination current.	$J_{\text{SC}}, J_0^{\text{rad}}$
3 Growth condition	In thermal equilibrium, materials can exchange atoms with their external environment. The available set of chemical potentials can be calculated using <code>CPLAP</code> . <sup>1</sup>	$\mu_i$
4 Formation energy	For a set of elemental chemical potentials (step 3), the formation energy of a defect is given by a function of the Fermi level. The difference in energies between charge state provides the thermal charge-transition level.	$E_f, E_T$
5 Configuration coordinate	The potential energy surface between equilibrium structures with different charge states can be mapped using <code>CarrierCapture.jl</code> . <sup>2</sup>	
5 Capture coefficient	The capture coefficient can be calculated by solving the 1D Schrödinger equations for the vibrations of defects (step 5) and overlap integrals between their wave functions, which can be performed using <code>CarrierCapture.jl</code> . <sup>2</sup>	$C_{n/p}$
6 Self-consistent Fermi level	The formation energy is a function of the Fermi-level (step 4) while the Fermi level is a function of the concentration of defects. The <code>SC-FERMI</code> code <sup>3</sup> can find the self-consistent Fermi level that satisfies the charge neutrality condition where a net charge of defects (step 4) is equal to a net charge of carriers (step 1).	$E_F, N_T, n_0, p_0$
7 SRH recombination rate	For given carrier and defect concentrations (step 6), defect levels (step 4), and the capture coefficient (step 5), the steady-state recombination rate can be calculated using Shockley-Read-Hall statistics.	$R_{\text{SRH}}$
8 Device simulation	The current-voltage relation can be calculated by combining the radiative limit (step 2) with the nonradiative recombination rate (step 7).	$J = J(V)$
9 Trap-limited conversion efficiency	The efficiency is given by the current times the voltage (step 8) divided by the illumination power. The maximum efficiency can be found along the voltage.	$\eta$

TABLE S1. The physical processes considered when calculating the trap-limited conversion efficiency (TLC) are shown in Fig. S1 and Fig. 1 in the main text. The detailed computational steps and calculated parameters are described. The numbered steps are the same as in Fig. 1 in the main text.

### Computational details

The total energy of pristine and defective crystals was calculated from DFT<sup>4,5</sup> using the projector-augmented wave (PAW) method<sup>6</sup> and the hybrid exchange-correlation functional of Heyd-Scuseria-Ernzerhof (HSE06),<sup>7</sup> as implemented in `VASP`.<sup>8</sup> We used a value of screened exact exchange that reproduces the experimental band gap of kesterites. The wave functions were expanded in plane waves up to an energy cutoff of 380 eV. The all-electron wave functions were derived from the pseudo wave functions and atom-centered partial waves in the PAW method, and the overlap integrals were performed in real space using `pawpyseed`<sup>9</sup> to calculate the electron-phonon coupling outlined by Alkauskas *et al.*<sup>10</sup>. A Monkhorst-Pack  $k$ -mesh<sup>11</sup> with a grid spacing less than  $2\pi \times 0.03 \text{ \AA}^{-1}$  was used for Brillouin zone integration. The atomic coordinates were optimized until the residual forces were less than  $0.01 \text{ eV/\AA}$ . The lattice vectors were relaxed until residual stress was below 0.5 kbar. For defect formation, a  $2 \times 2 \times 2$  supercell expansion (64 atoms) of the conventional cell was employed.

#### First-principles theory for nonradiative carrier capture:

*Configuration coordinate:* We described the degree of deformation using a one-dimensional configuration coordinate  $Q$  defined by

$$Q^2 = \sum_i m_i \Delta \mathbf{R}_i^2, \quad (\text{S1})$$

where  $m_i$  and  $\Delta \mathbf{R}_i$  are the atomic mass and the displacement vector from the equilibrium position of atom  $i$ , respectively. The vibrational wave function of excited ( $\xi_{cm}$ ) and ground ( $\xi_{tn}$ ) states, and associated eigen-energies  $\epsilon_{cm}$  and  $\epsilon_{tn}$  were obtained by solving the one-dimensional Schrödinger equation for potential energy surfaces around the equilibrium geometries.

*Electron-phonon coupling:* The electron-phonon coupling matrix elements are calculated based on the static approximation. We calculated the overlap of Kohn-Sham orbitals of the localized defect state and the delocalized band edges  $\langle \psi_t(Q) | \psi_c \rangle$ , and their gradient changes in the the configuration coordinate. The electron-phonon coupling matrix element is given by

$$\begin{aligned} W_{ct} &= \langle \psi_t | \partial H / \partial Q | \psi_c \rangle \\ &= \frac{d}{dQ} \langle \psi_t(Q) | \psi_c \rangle \end{aligned}$$

following the previous work of Alkauskas *et al.*<sup>2,10,12</sup>

*Sommerfeld factor:* The Coulomb interaction at temperature  $T$  between a carrier with charge  $q$  and a defect in a charge state  $Q$  is accounted by the Sommerfeld factor  $\langle s \rangle$ ;<sup>13,14</sup>

$$\langle s \rangle = \begin{cases} 4|Z|(\pi E_R/k_B T)^{\frac{1}{2}}, & \text{for } Z < 0 \\ 8/\sqrt{3}(\pi^2 Z^2 E_R/k_B T)^{\frac{2}{3}} \\ \times \exp(-3(Z^2 \pi^2 E_R/k_B T)^{\frac{1}{3}}), & \text{for } Z > 0, \end{cases} \quad (\text{S2})$$

where  $k_B$  is the Boltzmann constant.  $E_R = m^* q^4 / (2\hbar^2 \varepsilon^2)$  is an effective Rydberg energy where  $m^*$  and  $\varepsilon$  are an effective mass of the carrier and a low-frequency dielectric constant, respectively. For an attractive center,  $Z = Q/q$  is negative, while  $Z$  is positive for a repulsive center.

Host	$E_{\text{gap}}$ (eV)	$\alpha$	$\varepsilon_{(x,y,z)}$	$m_e$	$N_V$ (cm <sup>-3</sup> )	$N_C$ (cm <sup>-3</sup> )
CZTS	1.50	0.253	(8.85, 8.85, 9.40)	0.14	$2.30 \times 10^{19}$	$2.49 \times 10^{18}$
CZTSe	1.10	0.268	(9.62, 9.62, 10.26)	0.11	$6.02 \times 10^{19}$	$7.48 \times 10^{16}$
CZGSe	1.36	0.278	(10.13, 10.13, 10.29)	0.13	$1.03 \times 10^{19}$	$1.30 \times 10^{17}$
AZTSe	1.35	0.309	(9.16, 9.16, 9.49)	0.13	$1.51 \times 10^{19}$	$7.87 \times 10^{17}$

TABLE S2. Calculated properties of the host materials considered in this study. We optimized the band gap  $E_{\text{gap}}$  by tuning the fraction of exact exchange  $\alpha$  to reproduce the experimental band gap.  $\varepsilon$  is the relative dielectric tensor used to calculate the Sommerfeld factor. The effective densities of hole ( $N_V$ ) and electron ( $N_C$ ) are calculated at 300 K using density of states  $D(E)$  and carrier densities ( $n_0$  and  $p_0$ ) determined from the self-consistent Fermi level determination (see text).

Host	Trap	$N_T$ (cm <sup>3</sup> )	$E_T$ (eV)	$E_b$ (meV)	$C_n$ (cm <sup>3</sup> s <sup>-1</sup> )	$\sigma_n$ (cm <sup>2</sup> )
CZTS	V <sub>Cu</sub> (-/0)	$3.31 \times 10^{18}$ ( $5.40 \times 10^{18}$ )	0.04			
CZTS	Cu <sub>Zn</sub> (-/0)	$1.07 \times 10^{20}$ ( $1.67 \times 10^{20}$ )	0.19			
CZTS	Sn <sub>Zn</sub> (+/2+)	$1.32 \times 10^{14}$ ( $5.03 \times 10^{13}$ )	0.61	262	$1.19 \times 10^{-7}$	$1.19 \times 10^{-14}$
CZTS	Sn <sub>Zn</sub> -Cu <sub>Zn</sub> (0/+)	$5.27 \times 10^{15}$ ( $3.21 \times 10^{15}$ )	0.90	34	$1.47 \times 10^{-6}$	$1.47 \times 10^{-13}$
CZTSe	V <sub>Cu</sub> (-/0)	$8.52 \times 10^{19}$ ( $1.09 \times 10^{20}$ )	0.07			
CZTSe	Cu <sub>Zn</sub> (-/0)	$1.36 \times 10^{20}$ ( $1.69 \times 10^{20}$ )	0.21			
CZTSe	Sn <sub>Zn</sub> (+/2+)	$3.19 \times 10^{14}$ ( $1.97 \times 10^{14}$ )	0.48	69	$9.29 \times 10^{-7}$	$9.29 \times 10^{-14}$
CZTSe	V <sub>Se</sub> -Cu <sub>Zn</sub> (-/0)	$8.80 \times 10^{11}$ ( $1.11 \times 10^{12}$ )	0.16	152	$4.88 \times 10^{-10}$	$4.88 \times 10^{-17}$
CZGSe	V <sub>Cu</sub> (0/-)	$3.43 \times 10^{19}$ ( $5.55 \times 10^{19}$ )	0.03			
CZGSe	Cu <sub>Zn</sub> (0/-)	$9.70 \times 10^{19}$ ( $1.37 \times 10^{20}$ )	0.20			
CZGSe	Ge <sub>Zn</sub> (+/2+)	$6.97 \times 10^{14}$ ( $2.74 \times 10^{14}$ )	0.43	620	$9.97 \times 10^{-12}$	$9.29 \times 10^{-19}$
CZGSe	Ge <sub>Zn</sub> -Cu <sub>Zn</sub> (0/+)	$2.03 \times 10^{17}$ ( $1.12 \times 10^{17}$ )	0.87	71	$2.38 \times 10^{-8}$	$2.38 \times 10^{-15}$
AZTSe	V <sub>Ag</sub> (0/-)	$3.14 \times 10^{17}$ ( $6.26 \times 10^{18}$ )	0.25			
AZTSe	Ag <sub>Zn</sub> (0/-)	$7.78 \times 10^{18}$ ( $9.71 \times 10^{19}$ )	0.55			
AZTSe	Sn <sub>Zn</sub> (+/2+)	$1.99 \times 10^{14}$ ( $1.90 \times 10^{12}$ )	0.83	111	$4.64 \times 10^{-7}$	$4.64 \times 10^{-14}$

TABLE S3. Properties of dominant acceptors and recombination centers in kesterites. The concentration of traps  $N_T$  are calculated at the optimal growth conditions (see main text).  $N_T$  with the doping during the growth is shown in the parentheses. The electron-capture coefficient  $C_n$  and cross section  $\sigma_n$  are calculated at 300 K, assuming the thermal velocity  $v_{\text{th}} = 10^7$  cm s<sup>-1</sup>.

- 
- \* a.walsh@imperial.ac.uk
- <sup>1</sup> J. Buckeridge, D. O. Scanlon, A. Walsh and C. R. A. Catlow, *Comput. Phys. Commun.*, 2014, **185**, 330.
  - <sup>2</sup> *CarrierCapture*, <https://github.com/WMD-group/CarrierCapture.jl>, Accessed: 2019-10-26.
  - <sup>3</sup> J. Buckeridge, *Comput. Phys. Commun.*, 2019, **244**, 329–342.
  - <sup>4</sup> P. Hohenberg and W. Kohn, *Phys. Rev.*, 1964, **136**, B864.
  - <sup>5</sup> W. Kohn and L. J. Sham, *Phys. Rev.*, 1965, **140**, A1133.
  - <sup>6</sup> P. E. Blöchl, *Phys. Rev. B*, 1994, **50**, 17953.
  - <sup>7</sup> J. Heyd, G. E. Scuseria and M. Ernzerhof, *J. Chem. Phys.*, 2003, **118**, 8207.
  - <sup>8</sup> G. Kresse and D. Joubert, *Phys. Rev. B*, 1999, **59**, 1758.
  - <sup>9</sup> K. Bystrom, D. Broberg, S. Dwaraknath, K. A. Persson and M. Asta, *Paupyseed: Perturbation-extrapolation Band Shifting Corrections for Point Defect Calculations*, 2019.
  - <sup>10</sup> A. Alkauskas, Q. Yan and C. G. Van de Walle, *Phys. Rev. B*, 2014, **90**, 075202.
  - <sup>11</sup> H. J. Monkhorst and J. D. Pack, *Phys. Rev. B*, 1976, **13**, 5188.
  - <sup>12</sup> S. Kim, S. N. Hood and A. Walsh, *Phys. Rev. B*, 2019, **100**, 041202(R).
  - <sup>13</sup> R. Pässler, *Phys. Status Solidi B*, 1976, **78**, 625–635.
  - <sup>14</sup> P. T. Landsberg, *Recombination in Semiconductors*, Cambridge University Press, Cambridge, UK, 2009.